



# Source Population and Acceleration Location of Suprathermal Heavy Ions in Corotating Interaction Regions

R. J. Filwett<sup>1,2</sup>, M. I. Desai<sup>1,2</sup>, M. A. Dayeh<sup>2</sup>, and T. W. Broiles<sup>2</sup>

<sup>1</sup>University of Texas at San Antonio, San Antonio, TX, USA

<sup>2</sup>Southwest Research Institute, San Antonio, TX, USA

Received 2016 July 28; revised 2017 January 23; accepted 2017 January 25; published 2017 March 21

## Abstract

We have analyzed the  $\sim 20\text{--}320$  keV nucleon<sup>-1</sup> suprathermal (ST) heavy ion abundances in 41 corotating interaction regions (CIRs) observed by the *Wind* spacecraft from 1995 January to 2008 December. Our results are: (1) the CIR Fe/CNO and NeS/CNO ratios vary with the sunspot number, with values being closer to average solar energetic particle event values during solar maxima and lower than nominal solar wind values during solar minima. The physical mechanism responsible for the depleted abundances during solar minimum remains an open question. (2) The Fe/CNO increases with energy in the 6 events that occurred during solar maximum, while no such trends are observed for the 35 events during solar minimum. (3) The Fe/CNO shows no correlation with the average solar wind speed. (4) The Fe/CNO is well correlated with the corresponding upstream  $\sim 20\text{--}320$  keV nucleon<sup>-1</sup> Fe/CNO and not with the solar wind Fe/O measured by *ACE* in 31 events. Using the correlations between the upstream  $\sim 20\text{--}40$  keV nucleon<sup>-1</sup> Fe/CNO and the  $\sim 20\text{--}320$  keV nucleon<sup>-1</sup> Fe/CNO in CIRs, we estimate that, on average, the ST particles traveled  $\sim 2$  au along the nominal Parker spiral field line, which corresponds to upper limits for the radial distance of the source or acceleration location of  $\sim 1$  au beyond Earth orbit. Our results are consistent with those obtained from recent surveys, and confirm that CIR ST heavy ions are accelerated more locally, and are at odds with the traditional viewpoint that CIR ions seen at 1 au are bulk solar wind ions accelerated between 3 and 5 au.

**Key words:** acceleration of particles – shock waves – solar wind – Sun: abundances – Sun: heliosphere

## 1. Introduction

Corotating interaction regions (CIRs) are the main producer of energetic particles in the inner heliosphere during solar minimum (e.g., McDonald et al. 1976; Van Hollebeke et al. 1978; Richardson et al. 1993). CIRs form when streams of fast wind flowing from coronal holes overtake the slow solar wind in front of them. The solar rotation causes these different speed plasmas to become radially aligned and interact (e.g., Gosling 1996). This interaction creates a compression region that corotates with the Sun and can strengthen to form shocks that accelerate particles. Although only 31% of CIRs observed at 1 au have shocks (Jian et al. 2006), energetic particle enhancements are consistently observed near CIRs regardless of the presence of a shock. The classical view is that these enhancements arise from the Sunward propagation of particles accelerated at CIR shocks between  $\sim 3\text{--}5$  au (Fisk & Lee 1980). It is also expected that as these particles move into the inner heliosphere they will lose energy through adiabatic deceleration as they propagate against the outflowing solar wind (SW). This deceleration is expected to produce a spectral rollover below  $\sim 500$  keV nucleon<sup>-1</sup> near 1 au. This rollover has not been observed as predicted (Mason et al. 1997); instead CIR particle spectra are seen as continuous power laws down to  $< 100$  keV nucleon<sup>-1</sup> (Mason et al. 1997, 2008; Chotoo et al. 2000).

This discrepancy between theoretical predictions and observations has given rise to the alternate possibility that CIR-associated suprathermal ions below  $\sim 1$  MeV nucleon<sup>-1</sup> are accelerated closer to 1 au. This notion has now been confirmed by a number of studies. Chotoo et al. (2000) showed that  $0.01\text{--}0.5$  MeV nucleon<sup>-1</sup> H<sup>+</sup>, He<sup>+</sup>, and He<sup>++</sup> typically peaked in the compressed solar wind between the CIR stream interface and compression region trailing edge. Kucharek et al.

(2003) found the  $\sim 0.25\text{--}0.8$  MeV nucleon<sup>-1</sup> He<sup>+</sup>/He<sup>++</sup> ratios to be enhanced in nearly all CIRs observed at 1 au from 1998 to 2000; they interpreted this as evidence for local acceleration of interplanetary He<sup>+</sup>. Ebert et al. (2012) suggested that particles  $< 1$  MeV nucleon<sup>-1</sup> in CIRs were accelerated locally, while those  $> 1$  MeV nucleon<sup>-1</sup> are accelerated by CIR-driven shocks beyond 1 au. Thus, it is likely that CIR-associated acceleration processes begin even before shocks form. For this reason, Giacalone et al. (2002) suggested a mechanism that could accelerate low-energy particles in regions of gradual compression where the particles gain energy by scattering between converging centers and repeatedly sampling the SW speed gradient across the size of the compression in a process similar to diffusive shock acceleration at a quasi-parallel shock. Similarly, Chen et al. (2015) modeled gradual compression of pickup ions (PUIs) in CIRs without shocks and found significant acceleration at or inside of 1 au. These results indicate that compressions may play a critical role in local acceleration. Questions still remain as to where the most pronounced particle acceleration is occurring and what the relative acceleration efficiencies of gradual compressions compared to shocks are.

The differences between this study and previous CIR heavy ion studies, such as Mason et al. (2008), is that we use local compression regions that were identified from the plasma and magnetic field data (Broiles et al. 2012), and so not all events may be CIRs, but they are rather better defined as stream interaction regions (Jian et al. 2006). Furthermore, we consider a lower energy range than Bučik et al. (2012) who reported suprathermal Fe/O abundances for 137 keV nucleon<sup>-1</sup>. In this study, we examine suprathermal (ST) heavy ions between  $\sim 20\text{--}320$  keV nucleon<sup>-1</sup> in 41 local compression regions to further understand the source location and mechanisms of particle acceleration.

## 2. Instrumentation, Event Selection, and Data Analysis

### 2.1. Instrumentation

We use data obtained by the Suprathermal Energetic Particle (STEP) instrument, which is part of the Energetic Particles: Anisotropy, Composition, and Transport (EPACT) investigation (von Rosenvinge et al. 1995) on board the *Wind* spacecraft, launched in 1994 November (von Rosenvinge et al. 1995). STEP uses time-of-flight versus residual energy measurements to identify elements over the He-Fe in the  $\sim 0.02\text{--}2\text{ MeV nucleon}^{-1}$  energy range in two identical telescopes, with a geometric factor of  $0.4\text{ cm}^2\text{ sr}$  and a rectangular field of view with an angular acceptance of  $44^\circ$  in azimuth and  $17^\circ$  in polar angle. STEP comprises two telescopes with a sampling region  $\pm 35^\circ$  from the ecliptic on the spinning spacecraft; for this investigation we only use data obtained by Telescope 1. We also use solar wind data from the Solar Wind Ion Composition Spectrometer (SWICS) instrument (Gloeckler et al. 1992) on the *ACE* spacecraft. SWICS determines the mass and ionic charge state composition of solar wind ions; for this study we use the 1 hr averaged Fe/O ratios. Due to the later launch of *ACE*, the solar wind Fe/O from *ACE*/SWICS is not available for all events studied; 31 of the 41 events examined had coverage by both *Wind* and *ACE*.

### 2.2. Event Selection

We start with the list of compression regions observed at 1 au between 1995 January 1 and 2008 December 31 identified by Broiles et al. (2012) using plasma and magnetic field properties. For this study we selected 41 out of the original 153 events from the Broiles et al. (2012) list. 105 events were excluded for a variety of reasons; in 75 events, the particle time-intensity profiles were atypical of CIR events because they exhibited velocity dispersion typical of solar energetic particle (SEP) events that are injected near the Sun (e.g., Mazur et al. 1999), the Broiles et al. (2012) time intervals included multiple and overlapping CIRs, or the plasma signatures of the CIRs did not overlap with increases in the particle intensities. 27 events had strong contributions from upstream events, which enhanced the particle intensities at energies below  $\sim 80\text{ keV nucleon}^{-1}$  (e.g., Desai et al. 2000). The upstream events were identified by comparing the intensities at  $\sim 20\text{--}40\text{ keV nucleon}^{-1}$  and  $\sim 160\text{--}320\text{ keV nucleon}^{-1}$  in each individual event. Furthermore, 10 events were excluded because the  $\sim 160\text{--}320\text{ keV nucleon}^{-1}$  Fe/CNO ratio had relative uncertainty  $>35\%$ . A complete list of the 41 events studied here is given in Table 1; events in the Mason et al. (2008) study are also identified. In 28 cases, we modified the event start or stop times from the original Broiles et al. (2012) survey to achieve the following: (1) include all ST particles associated with the CIR event; (2) exclude unrelated trailing events, such as potential coronal mass ejections that overlapped with the trailing boundary of the CIR event, and (3) remove upstream events that originate from the bow shock and contribute to the ion intensity or fluences at lower energies.

Figure 1 shows hourly averages of (a) the  $\sim 20\text{--}320\text{ keV nucleon}^{-1}$  ST ion intensities, (b) the solar wind speed, (c) magnetic field strength, and (d) the solar wind proton density for event number 14 in Table 1. The 13 day time interval shown (2000 March 17–March 30) encompasses the CIR duration (black vertical lines) as identified by Broiles et al.

(2012) along with data obtained a few days surrounding the event. This CIR displays particle, plasma, and field signatures that are typical of previously reported CIR observations at 1 au (e.g., Jian et al. 2006). Specifically, the peaks in the magnetic field strength and the plasma density that define the compression region are seen on 2000 March 22 10:55 UT prior to the arrival of the high speed stream at 2000 March 22 18:56 UT. In addition, the particle intensities peak in the high speed stream, as reported, for example, by Mason et al. (1997). Figure 1 also shows the corresponding upstream interval we use in this study to obtain the solar wind Fe/O and the suprathermal Fe/CNO ratios (see Section 3.6 for further details), which serve as proxies for potential seed populations for the CIR.

### 2.3. Calculation of Abundance Ratios

The elemental abundance ratios provided in this study were calculated using the event-integrated fluences during the sampling intervals listed in Table 1 in four different energy bands, namely  $\sim 20\text{--}40$ ,  $\sim 40\text{--}80$ ,  $\sim 80\text{--}160$ , and  $\sim 160\text{--}320\text{ keV nucleon}^{-1}$ . We do not include the  $\sim 20\text{--}40\text{ keV nucleon}^{-1}$  NeS/CNO in this study because STEP does not have sufficient mass resolution for NeS at these energies. The 41 events are separated into those that occurred during solar maximum and those that occurred during a solar activity phase more representative of solar minimum. Solar maximum is defined as the time period when average monthly smoothed sunspot number is equal to or greater than 75, and solar minimum includes time periods from 1995 January 1 to 2008 December 1 when the sunspot number falls below 75. Solar maximum is from 1998 December through 2003 February 1 and includes 6 events; the remaining 35 events occur during solar minimum.

## 3. Properties of CIR Suprathermal Abundances

### 3.1. Solar Activity Dependence

We examine ST heavy ion abundances, their energy dependence, and trends with solar activity cycle over 14 years, covering all of solar cycle 23. Figure 2(a) shows the hourly averaged  $\sim 160\text{--}320\text{ keV nucleon}^{-1}$  CNO intensity measured over 14 years along with the corresponding hourly averaged intensity in the 41 events; blue circles: events in solar minimum; red squares: events during solar maximum. Figure 2(b) shows that the Fe/CNO varied with the sunspot number; see Figures 2(b) and (c). Up to the year 2000, the Fe/CNO in CIRs is well below that of the corresponding solar wind value; the Fe/CNO increases to values slightly below that of gradual SEPs between 2000 and 2003. We remark that this trend follows the sunspot number and is seen over the entire ST energy regime of  $\sim 20\text{--}320\text{ keV nucleon}^{-1}$  covered in this study.

### 3.2. Event Statistics

To obtain a clearer picture of the ST abundance trends, we study the event-to-event variations in abundance distributions, and event durations for the 41 events. Figure 3 shows the distribution of event durations; the mean duration is 2.96 days for all the events, with a mean of 2.66 days for solar minimum and 3.74 days for solar maximum. However, the 1-sigma uncertainties in the mean values make these differences insignificant. Furthermore, although the solar maximum events have higher Fe/CNO ratio, and slightly longer event durations,

**Table 1**  
Corotating Interaction Region Events Studied Here

Event Number (1)	Year (2)	Start Day and Time (3)		End Day and Time (4)		40–80 keV nucleon <sup>-1</sup>		Solar Wind Velocity (km s <sup>-1</sup> ) (8)
						Fe/CNO X 100 (6)	NeS/CNO X 100 (7)	
1	1995	Jan 28	17:54	Jan 31	3:36	4.0 ± 0.4	18.2 ± 1.0	661
2	1995	Apr 6	12:15	Apr 8	19:12	3.3 ± 0.1	12.2 ± 0.3	636
3	1995	Apr 26	12:54	Apr 28	0:00	4.1 ± 0.8	15.2 ± 2.0	613
4	1995	May 1	20:51	May 4	10:48	2.1 ± 0.2	14.0 ± 0.7	696
5	1995	May 23	14:26	May 26	14:24	3.0 ± 0.4	15.8 ± 1.1	568
6	1995	May 29	7:12	Jun 1	7:12	10.6 ± 0.1	17.8 ± 0.2	652
7	1995	Jun 18	21:23	Jun 21	0:00	2.0 ± 0.3	15.1 ± 1.0	654
8	1995	Jul 16	9:04	Jul 17	14:24	3.6 ± 0.6	13.8 ± 1.5	614
9	1995	Aug 7	9:11	Aug 10	2:24	3.0 ± 0.2	13.5 ± 0.4	564
10	1995	Dec 24	5:49	Dec 26	7:12	2.0 ± 0.1	12.4 ± 0.3	599
11 <sup>a</sup>	1998	Jul 15	16:23	Jul 20	23:48	1.5 ± 0.1	12.3 ± 0.4	550
12 <sup>a</sup>	1999	Dec 2	23:16	Dec 6	6:00	3.4 ± 0.1	21.1 ± 0.4	609
13 <sup>a</sup>	2000	Feb 5	14:49	Feb 7	18:00	6.9 ± 0.2	21.8 ± 0.6	630
14 <sup>a</sup>	2000	Mar 22	10:55	Mar 26	18:21	6.2 ± 0.2	21.5 ± 0.6	570
15	2002	Mar 3	13:38	Mar 11	6:37	16.7 ± 0.8	25.8 ± 1.5	584
16 <sup>a</sup>	2002	Nov 20	10:16	Nov 22	12:00	7.0 ± 0.2	20.1 ± 0.5	681
17	2002	Dec 14	2:28	Dec 17	0:31	15.4 ± 1.7	39.6 ± 4.3	480
18 <sup>a</sup>	2004	Nov 20	7:12	Nov 21	18:43	5.8 ± 0.2	24.9 ± 0.5	554
19	2005	Jan 11	7:12	Jan 13	0:00	3.0 ± 0.3	22.7 ± 1.0	645
20	2005	Apr 3	15:43	Apr 6	3:51	1.6 ± 0.3	16.7 ± 1.2	591
21	2005	Jun 4	10:07	Jun 10	12:08	15.7 ± 0.8	46.1 ± 1.9	454
22	2005	Jun 23	1:56	Jun 27	8:08	5.2 ± 0.9	40.5 ± 3.3	522
23 <sup>a</sup>	2005	Oct 7	3:27	Oct 8	19:12	6.0 ± 0.2	20.8 ± 0.6	684
24	2005	Dec 18	20:19	Dec 22	10:10	15.1 ± 1.0	48.9 ± 2.5	513
25	2006	Jun 6	3:56	Jun 7	15:36	6.7 ± 0.9	26.9 ± 2.5	582
26	2006	Jul 30	22:30	Aug 4	11:38	4.3 ± 0.5	25.5 ± 1.7	571
27	2006	Aug 6	23:12	Aug 9	0:00	3.1 ± 0.3	21.2 ± 1.1	577
28	2006	Aug 26	23:58	Aug 28	2:24	9.4 ± 0.7	33.2 ± 1.8	594
29	2006	Sep 23	11:38	Sep 25	12:00	5.4 ± 0.2	21.6 ± 0.6	475
30	2006	Oct 19	23:18	Oct 24	14:24	5.7 ± 0.4	24.2 ± 1.0	552
31	2006	Nov 9	11:49	Nov 15	0:00	4.8 ± 0.3	23.0 ± 0.7	546
32	2007	Jan 27	21:36	Jan 20	9:36	3.6 ± 0.2	23.0 ± 0.7	582
33	2007	Feb 27	0:57	Mar 2	11:06	5.6 ± 0.7	22.2 ± 1.9	621
34	2007	May 7	7:23	May 11	2:32	5.6 ± 0.4	19.5 ± 1.0	582
35	2007	May 17	20:25	May 21	6:00	3.4 ± 0.7	23.7 ± 2.3	577
36	2007	Sep 27	10:55	Sep 30	0:00	1.5 ± 0.3	19.4 ± 1.4	611
37	2007	Dec 16	12:00	Dec 18	16:48	4.2 ± 0.3	20.5 ± 0.8	596
38	2008	Feb 9	17:35	Feb 11	18:28	6.4 ± 0.3	20.8 ± 0.7	668
39	2008	Mar 26	2:15	Mar 28	0:00	6.6 ± 1.4	23.4 ± 3.5	604
40	2008	Aug 8	19:48	Aug 11	14:24	4.7 ± 0.2	20.2 ± 0.4	610
41	2008	Nov 23	22:33	Nov 29	10:03	3.7 ± 0.2	18.6 ± 0.6	571

**Note.**

<sup>a</sup> Events included in study by Mason et al. (2008).

there is no general relation between event duration and abundance with solar activity. Figure 4 shows the distribution of Fe/CNO in all four energy ranges studied here. The figure shows that the abundance distributions are Gaussian in nature, with the Fe/CNO at each energy showing only slight variations in weighted mean or variance.

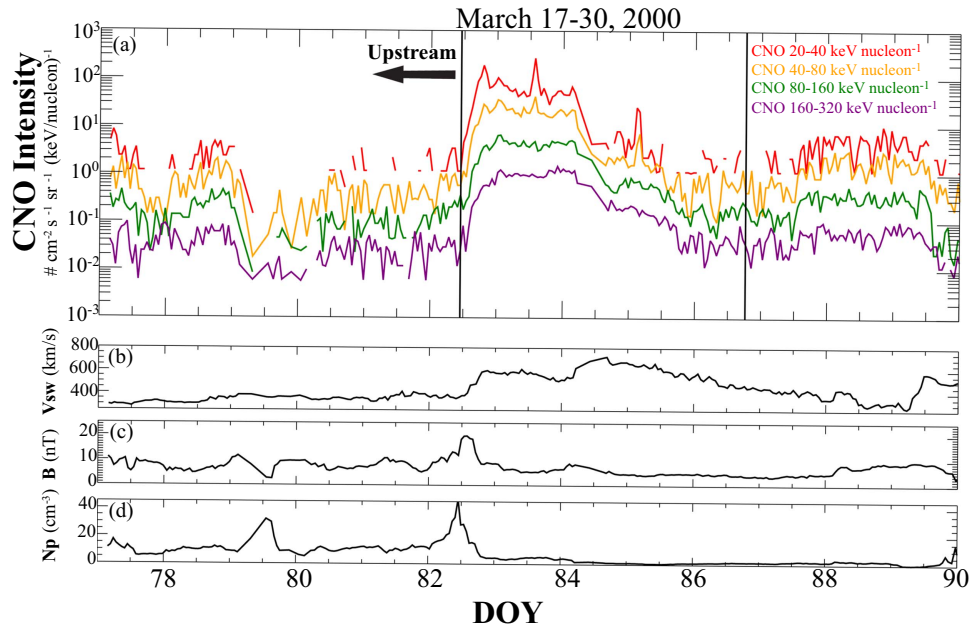
### 3.3. Event Fluences

Figure 5 shows scatter plots of the fluences for NeS versus CNO and Fe versus CNO at  $\sim 20\text{--}40$  keV nucleon<sup>-1</sup> and  $\sim 160\text{--}320$  keV nucleon<sup>-1</sup>. On average, the fluences during solar maximum CIRs are higher for Fe and NeS at both energies. The NeS versus CNO fluences are well constrained

within the lines of constant abundance of 0.1 and 1.0. The Fe versus CNO fluences point to Fe/CNO ratios below  $\sim 0.1$ , with those seen during solar maximum being larger, particularly at  $\sim 160\text{--}320$  keV nucleon<sup>-1</sup>.

### 3.4. Energy Dependence of Fe/CNO

In Figure 6, we examine the energy dependence of Fe/CNO and NeS/CNO ratio in CIRs. The Fe/CNO abundance ratio is slightly above one-to-one at all energies with an average ratio of 1.39 for  $\sim 40\text{--}80$  keV nucleon<sup>-1</sup> versus  $\sim 20\text{--}40$  keV nucleon<sup>-1</sup> and 1.48 at  $\sim 160\text{--}320$  keV nucleon<sup>-1</sup> versus  $\sim 20\text{--}40$  keV nucleon<sup>-1</sup>. However, this increase is within the standard error of the mean. For solar maximum events, shown



**Figure 1.** Particle, plasma, and magnetic field profiles for event number 14 listed in Table 1. (a) shows the CNO intensity at  $\sim 20$ – $40$ ,  $\sim 40$ – $80$ ,  $\sim 80$ – $160$ , and  $\sim 160$ – $320$  keV nucleon $^{-1}$ , the vertical black lines indicate the defined start and stop times for the event. Panels (b), (c), and (d) show the associated solar wind speed, interplanetary magnetic field strength, and solar wind proton density, respectively.

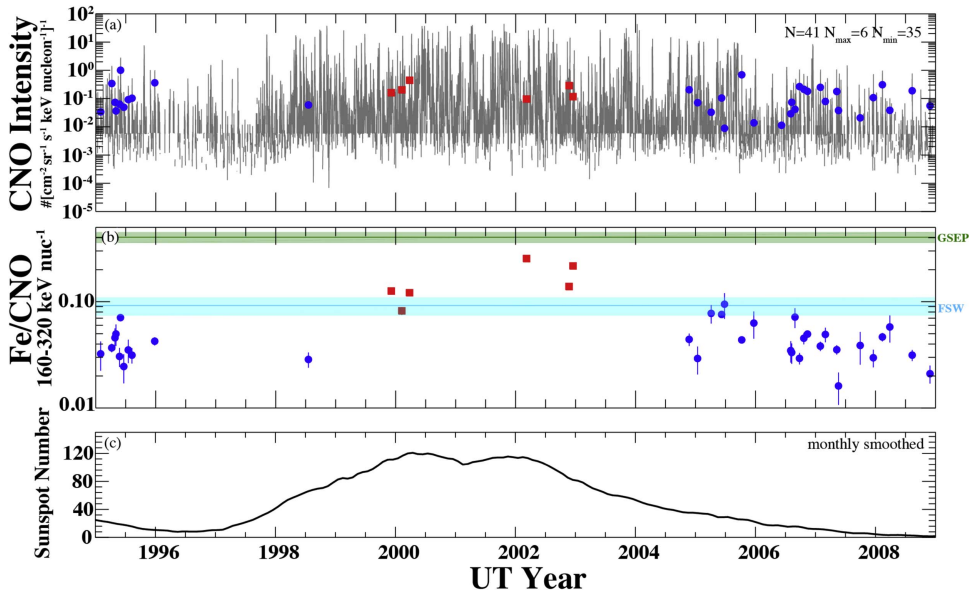


**Figure 2.** (a) Hourly averaged CNO intensity at  $\sim 160$ – $320$  keV nucleon $^{-1}$  (gray) over the total timespan of this study and the event-averaged (symbols) intensity for each of the corotating interaction regions (CIRs) in this study, showing their relative distributions over the solar cycle. (b) The Fe/CNO abundance at  $\sim 160$ – $320$  keV nucleon $^{-1}$  for each event vs. time. Also shown are the average abundances for gradual SEPs (Desai et al. 2006b), and fast solar wind (FSW) (von Steiger et al. 2000), with the width of the line representing the uncertainties in the abundances. The red squares indicate events that took place during solar maximum, and the blue circles show those that occurred during solar minimum. (c) The monthly averaged smoothed sunspot number.

in red, the average Fe/CNO ratio shows a factor of  $\sim 1.8$  increase with increasing energy, but this trend is not seen for the solar minima events. The NeS/CNO does not show an apparent trend with energy either during solar maximum or solar minimum. In summary, there are no clear increases for either Fe/CNO or NeS/CNO across the energy range studied, except the abundances in solar maximum CIRs show a consistent increase with energy. Table 2 provides the weighted mean of Fe/CNO and NeS/CNO for solar minimum and solar maximum events. As pointed out in Figures 2 and 6, the

Fe/CNO in CIRs during solar maximum is markedly larger compared with the corresponding Fe/CNO for events during solar minima.

### 3.5. Solar Wind Speed Versus Abundances

In Figure 7 we examine the relationship between SW speed and the  $\sim 160$ – $320$  keV nucleon $^{-1}$  Fe/CNO ratio for all events. The figure shows that the Fe/CNO does not exhibit a statistically significant correlation ( $p \leq 0.01$ ) with SW speed.

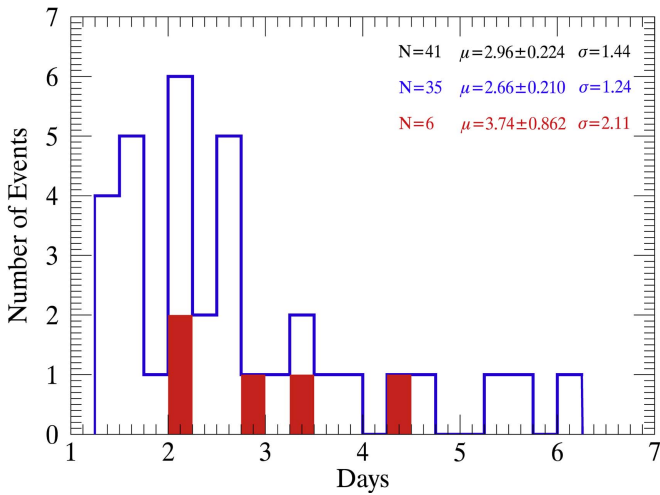


**Figure 3.** Distribution of the duration of solar minima and maxima CIR events. The distribution for solar minimum events is plotted in blue and solar maximum in red. The mean, standard error of the mean, standard deviation, and number of events are given for all events (black), solar maxima (red), and solar minima (blue).

There was no statistically significant relationship seen for Fe/CNO or NeS/CNO with solar wind speed at any energy considered in this study.

### 3.6. Correlation with Upstream SW and ST Abundances

We now study the relationship between the CIR ST abundances and the corresponding abundances measured in the upstream SW and ST Fe/CNO. Following the approach of Mason et al. (2008), who studied the correlation between  $\sim 320\text{--}450$  keV nucleon $^{-1}$  CIR Fe/O and the upstream SW Fe/O, we identified the time of maximum correlation for both the ST Fe/CNO and SW Fe/O upstream. In their survey, Mason et al. (2008) used upstream time intervals equal to those of the duration of the CIR, which varied from 1.25 to 3.5 days. We point out that the Mason et al. (2008) durations are much shorter than the average event duration in this study (mean duration 2.96 days, see Figure 3).

We calculated the Spearman correlation coefficient between the event and upstream abundances. The Spearman correlation is a nonparametric measure of rank correlation; it evaluates the monotonic relationship between two variables. Spearman’s correlation is useful for fitting functions, which may or may not have a strictly linear relationship; it also has less sensitivity to strong outliers that are in the tail of both distributions when compared to common linear fitting functions such as the Pearson correlation coefficient. The goodness of fit for the correlation is given by  $r$ , and the significance level, or probability that the variables are randomly related, by  $p$ . We assume that a given correlation coefficient is statistically significant if the corresponding  $p$  value  $\leq 0.01$ . We calculated the coefficient for each 1 hr interval over a period of 240 hr immediately preceding the start of each event. Other time intervals (e.g., 6, 12, 18, and 24 hr) were also examined, and we chose 18 hr because shorter time intervals did not converge to a smooth probability with time; they instead displayed random noise due to low statistics. Longer time averages tended to smooth over variations in the correlation coefficients and their probabilities.

We correlated the CIR Fe/CNO abundances with the upstream SW Fe/O in all four energy ranges, and the upstream ST Fe/CNO energies with all energies at equal or lower energies than that used for the CIR STs. Figure 8 shows the 18 hr averaged abundances for each event for two of the upstream correlations. The correlation coefficient and significance values are also given. These 18 hr trends start to give an indication of how the correlation varies with time. These figures clearly show that the  $\sim 20\text{--}40$  keV nucleon $^{-1}$  Fe/CNO in CIRs is strongly correlated with the upstream ST Fe/CNO but not with the SW Fe/O ratio.

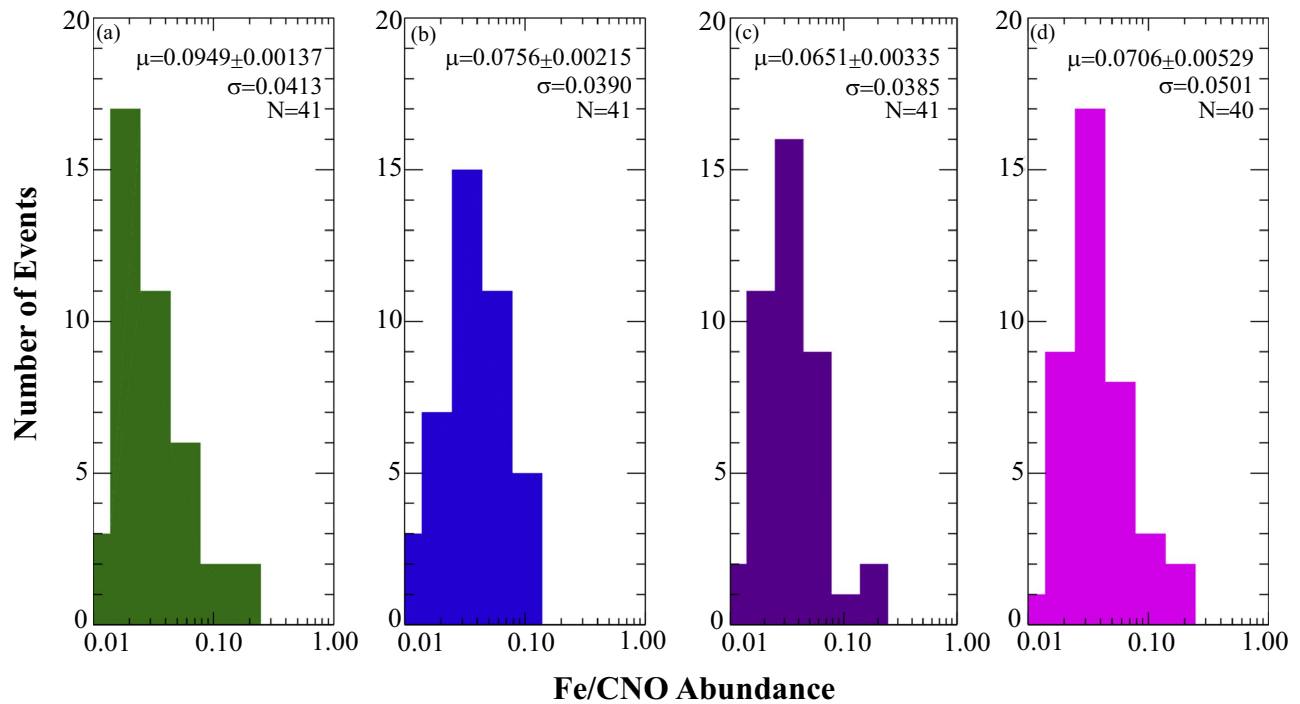
Figure 9 shows two examples of values of the upstream correlation coefficients with time; the  $\sim 20\text{--}40$  keV nucleon $^{-1}$  CIR Fe/CNO versus the  $\sim 20\text{--}40$  keV nucleon $^{-1}$  upstream Fe/CNO (solid line) and the upstream SW Fe/O (dashed line). These are the same two examples as in Figure 8 but now extended to 10 days upstream. Figure 9 shows that the upstream ST Fe/CNO ratio is better correlated with the CIR Fe/CNO compared with the upstream SW Fe/O as demonstrated by the higher correlation coefficient  $r = 0.55$ ,  $p = 1.87 \times 10^{-4}$  from 54 to 71 hr and  $r = 0.41$ ,  $p = 0.011$  from 90 to 107 hr, respectively. This shows that not only is the upstream ST Fe/CNO better correlated with the ST Fe/CNO in CIRs but also that the correlation with the upstream SW Fe/O is not statistically significant over the entire 10 day interval examined.

Figure 10 shows scatter plots for the 18 hr time interval with maximum correlation coefficients for the previously mentioned energy intervals, along with a linear fit to the data. Figure 10 exemplifies the pattern alluded to earlier, that the ST Fe/CNO ratios in CIRs and upstream are higher during solar maximum conditions compared with those seen during the solar minimum. Figures 10(a) and (c) show that the upstream Fe/O SW is well constrained within the nominal slow solar wind range of  $0.120 \pm 0.024$  (von Steiger et al. 2000). Except for the relationship between CIR and upstream SW abundances shown in Figure 10(c), all upstream correlations are statistically significant, with  $p$ -values  $\leq 0.01$ . Note that the upstream ST versus CIR abundance correlations remain statistically significant even when the 10 additional events that do not have SW data are removed, thus confirming that the correlations are indeed statistically significant.

Figure 11 summarizes our correlation analysis for the 18 hr averaged  $\sim 20\text{--}40$  keV nucleon $^{-1}$  upstream Fe/CNO (solid line) and the upstream SW Fe/O (dashed lines) when correlated with the event integrated CIR Fe/CNO at  $\sim 20\text{--}40$ ,  $\sim 40\text{--}80$ ,  $\sim 80\text{--}160$ , and  $\sim 160\text{--}320$  keV nucleon $^{-1}$ . The correlation coefficient and probability that the two variables being compared are a random distribution are shown. Figure 11 shows that the upstream SW Fe/O attains highest significance with  $\sim 20\text{--}40$  keV nucleon $^{-1}$  between 90 and 107 hr with a  $p$  value of 0.011, and except for  $\sim 40\text{--}80$  keV nucleon $^{-1}$  all correlations with upstream ST abundances are statistically significant. The correlation with STs at  $\sim 20\text{--}40$  keV nucleon $^{-1}$  in the upstream interval remains statistically significant up to 4.5 days prior to event start. The maximum correlation times shown in Figure 11 are summarized for all four energies in Table 3.

## 4. Discussion

We have analyzed the  $\sim 20\text{--}320$  keV nucleon $^{-1}$  ST heavy ion abundance in 41 CIRs observed during 1995–2008 using WIND/EPACT/STEP. Our results are:



**Figure 4.** The distribution of the Fe/CNO abundances for the four energy intervals in this study,  $\sim 20\text{--}40$  keV nucleon $^{-1}$  (green),  $\sim 40\text{--}80$  keV nucleon $^{-1}$  (blue),  $\sim 80\text{--}160$  keV nucleon $^{-1}$  (purple),  $\sim 160\text{--}320$  keV nucleon $^{-1}$  (magenta). The mean, standard error of the mean, standard deviation, and number of events are also shown.

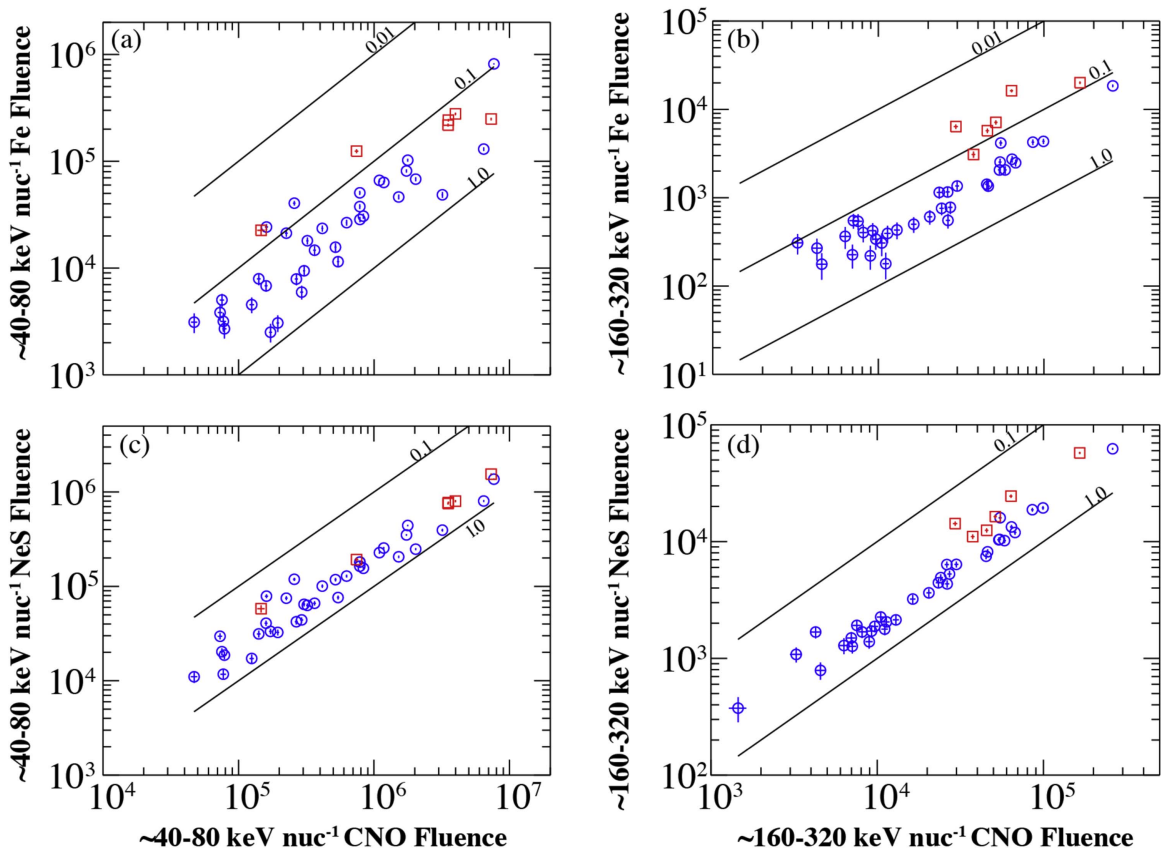


**Figure 5.** The event-integrated CNO fluences in each of the 41 events vs. Fe fluence at (a)  $\sim 40\text{--}80$  keV nucleon $^{-1}$  and (b)  $\sim 160\text{--}320$  keV nucleon $^{-1}$ , and also CNO fluences vs. NeS fluence at (c)  $\sim 40\text{--}80$  keV nucleon $^{-1}$  and (d)  $\sim 160\text{--}320$  keV nucleon $^{-1}$ . Lines of constant abundance are also shown.

**Table 2**  
Mean Abundance of Suprathermal Heavy Ions in CIR Events

Energy	All Events		Solar Minimum		Solar Maximum	
	Fe/CNO	NeS/CNO	Fe/CNO	NeS/CNO	Fe/CNO	NeS/CNO
20–40 keV nucleon <sup>-1</sup>	0.0949 ± 0.00137 $\sigma = 0.0413$	...	0.0410 ± 0.00129 $\sigma = 0.0198$	...	0.168 ± 0.00286 $\sigma = 0.0475$	...
40–80 keV nucleon <sup>-1</sup>	0.0756 ± 0.00215 $\sigma = 0.0390$	0.264 ± 0.00622 $\sigma = 0.0846$	0.0621 ± 0.00222 $\sigma = 0.0329$	0.254 ± 0.00624 $\sigma = 0.0864$	0.137 ± 0.00186 $\sigma = 0.0545$	0.320 ± 0.00610 $\sigma = 0.0742$
80–160 keV nucleon <sup>-1</sup>	0.0651 ± 0.00335 $\sigma = 0.0385$	0.222 ± 0.00763 $\sigma = 0.0686$	0.0506 ± 0.00330 $\sigma = 0.0224$	0.202 ± 0.00745 $\sigma = 0.0505$	0.147 ± 0.00373 $\sigma = 0.0615$	0.348 ± 0.00908 $\sigma = 0.0768$
160–320 keV nucleon <sup>-1</sup>	0.0706 ± 0.00527 $\sigma = 0.0501$	0.243 ± 0.0127 $\sigma = 0.0735$	0.0507 ± 0.00510 $\sigma = 0.0190$	0.228 ± 0.0126 $\sigma = 0.0495$	0.173 ± 0.00700 $\sigma = 0.0653$	0.366 ± 0.0128 $\sigma = 0.0764$

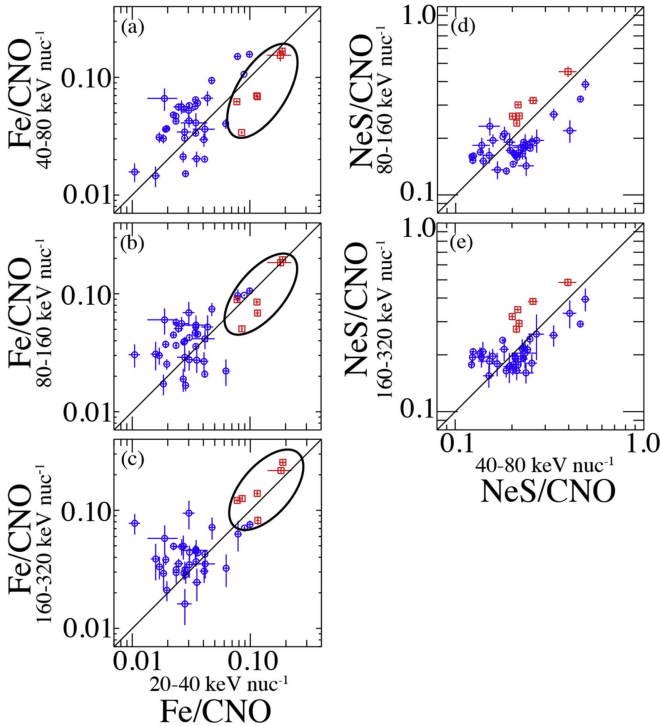


**Figure 6.** The  $\sim 20\text{--}40$  keV nucleon<sup>-1</sup> Fe/CNO and  $\sim 40\text{--}80$  keV nucleon<sup>-1</sup> NeS/CNO ratios compared to higher energy Fe/CNO and NeS/CNO, respectively. Left:  $\sim 20\text{--}40$  keV nucleon<sup>-1</sup> Fe/CNO plotted vs. (a)  $\sim 40\text{--}80$  keV nucleon<sup>-1</sup>, (b)  $\sim 80\text{--}160$  keV nucleon<sup>-1</sup>, and (c)  $\sim 160\text{--}320$  keV nucleon<sup>-1</sup> Fe/CNO. Right:  $\sim 40\text{--}80$  keV nucleon<sup>-1</sup> NeS/CNO plotted vs. (d)  $\sim 80\text{--}160$  keV nucleon<sup>-1</sup> and (e)  $\sim 160\text{--}320$  keV nucleon<sup>-1</sup> NeS/CNO. Six events during solar maximum are shown as red squares and 35 events during solar minimum as blue circles; the one-to-one line is also plotted for reference.

1. The  $\sim 20\text{--}320$  keV nucleon<sup>-1</sup> Fe/CNO and NeS/CNO ratios vary with the sunspot number, with larger values observed during solar maximum and lower abundances during solar minimum.
2. The Fe/CNO ratios show a slight increase with energy for the six events that occur during solar maximum; no energy dependent variations are seen for the CIR Fe/CNO ratios during solar minima.
3. The ST heavy ion abundances are not correlated with solar wind speed.
4. Suprathermal Fe/CNO in CIRs are well correlated with upstream suprathermal Fe/CNO and not with the upstream solar wind Fe/O.
5. The peak correlation time with upstream suprathermal Fe/CNO occurs between 45–99 hr for  $\sim 20\text{--}40$  keV nucleon<sup>-1</sup>

and 18–35 hr for  $\sim 160\text{--}320$  keV nucleon<sup>-1</sup> Fe/CNO in CIRs.

#### 4.1. Comparison with Previous CIR Abundance Studies

Previously, Bučik et al. (2012) studied ST heavy ions in CIRs and showed that elemental abundances tracked the solar cycle or solar activity. Specifically, Bučik et al. (2012) observed more than 50 CIRs using *STEREO* between 2007 and 2010 and found that the 137 keV nucleon<sup>-1</sup> Fe/O ratio varies significantly from event-to-event, but follows the preceding energetic particle activity. They also reported that the average elemental abundance over the 3 year period was similar to previously reported CIR abundances. Figure 12 shows the Fe/CNO ratio from Table 2 along with those obtained by Bučik et al. (2012) and by other CIR surveys. Previous studies of energetic particles in CIRs at  $\sim 0.385$  MeV nucleon<sup>-1</sup> and 5–12 MeV nucleon<sup>-1</sup> found Fe/O abundances of  $0.088 \pm 0.007$  and  $0.097 \pm 0.011$ , respectively (Reames 1995; Mason et al. 2008). Richardson et al. (1993) found that CIR abundances are ordered according to SW speed following the photospheric abundances, according to the first ionization potentials, which is not strictly related to solar activity. Mason et al. (2008) examined the relation between He/O, C/O, Mg/O, Si/O, and Fe/O and SW speed and found no significant correlation except for Si/O and Fe/O. Previously, Si/O and Fe/O had not been found to have a relationship with SW speed, and so although Mason et al. (2008) found correlation coefficients of  $r = 0.41$  and  $r = 0.47$ , respectively, they concluded that the dependence of these abundances on SW speed is unproven. Our results shown in Figure 7 indicate that there is no relation between SW speed and Fe/CNO abundance in CIRs, in agreement with the conclusions of Mason et al. (2008).

As shown in Table 2, the 41-event average abundance for Fe/CNO at all energies studied here is  $0.066 \pm 0.0065$ , and that for those reported by Mason et al. (1997) is Fe/O =  $0.08 \pm 0.03$ . The difference between the abundances in this study and Mason et al. (1997) is negligible when we examine the size of the reported errors. Furthermore, any difference in the values reported in this study may be lower than those obtained previously because our sampling time intervals include the onsets, peaks, and decay phases of the time-intensities during all CIR events rather than just the periods when the intensities peaked.

Figure 12 illustrates the energy dependence of the average abundances in CIRs. In Figure 12 we compare previously reported abundances from Mason et al. (1997), Reames (1995), Mason et al. (2008), and Bučik et al. (2012). We see little to no variation with energy, and all reported values are within, or

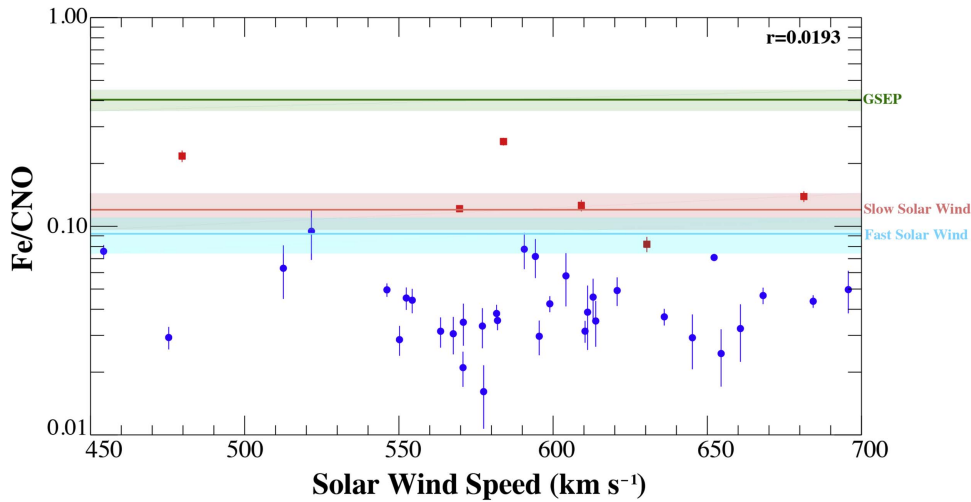


**Figure 7.** Fe/CNO abundance at  $\sim 160\text{--}320$  keV nucleon $^{-1}$  vs. solar wind speed. CIR events are shown as a function of solar activity: solar maximum events are red (squares), and solar minimum events are blue (circles). Average abundances (lines) with errors (shaded bars) are also shown for gradual SEPs (Desai et al. 2006b), slow solar wind, and fast solar wind (von Steiger et al. 2000).

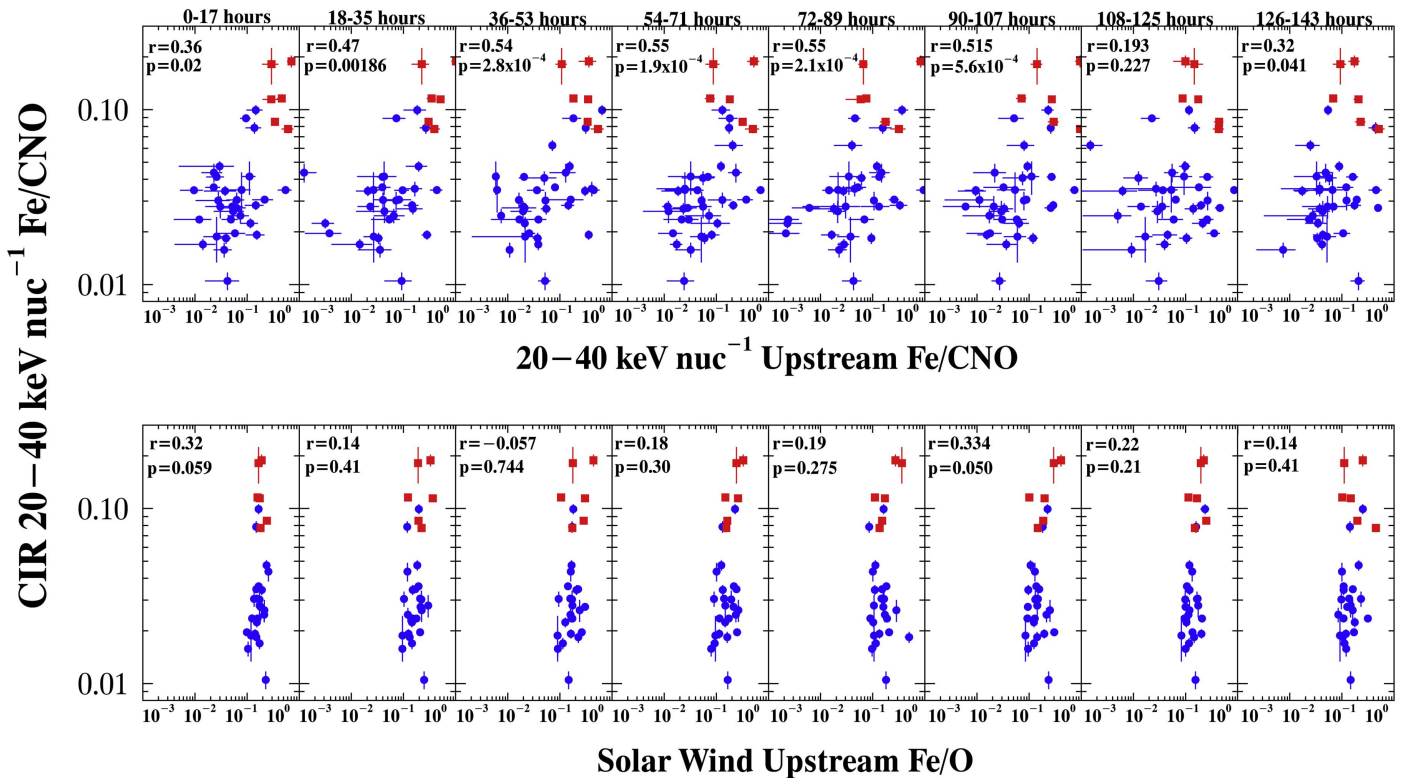


**Figure 8.** Scatter plots of CIRs STs vs. upstream STs (top) and vs. upstream solar wind (bottom) abundances during each 18 hr interval for the 6 days prior to the CIR start interval. The calculated Spearman correlation coefficient and  $p$  value are also given for each interval.

slightly below, the Fe/O ratio of the fast solar wind (von Steiger et al. 2000).

#### 4.2. Source Population

Table 2 and Figure 2(b) show a clear trend in the average ST heavy ion abundances in CIRs with solar cycle, with SEP-like abundances during solar maximum and depleted SW-like values during solar minimum. Possible explanations for these depleted values during solar minimum include  $M/Q$  dependent transport through the interplanetary medium, or acceleration mechanisms that accelerate ions with higher  $M/Q$  ratios less efficiently than

those with lower  $M/Q$  ratios, hence depleting the abundances of ions with higher  $M/Q$  ratios (Desai et al. 2003, 2009). The exact nature of the depletion mechanisms remains an open question that requires further work.

Similar solar cycle variations in the Fe/O abundances are also observed in the ST quiet-time populations (Desai et al. 2006b, 2009; Dayeh et al. 2009, 2016) and are interpreted as evidence of CIRs or SEPs contributing to ST material during different phases of solar activity. Thus, the abundance measurements of both quiet times and local compression regions studied here indicate the acceleration of ST material from prior solar and interplanetary activity, which varies with solar activity.

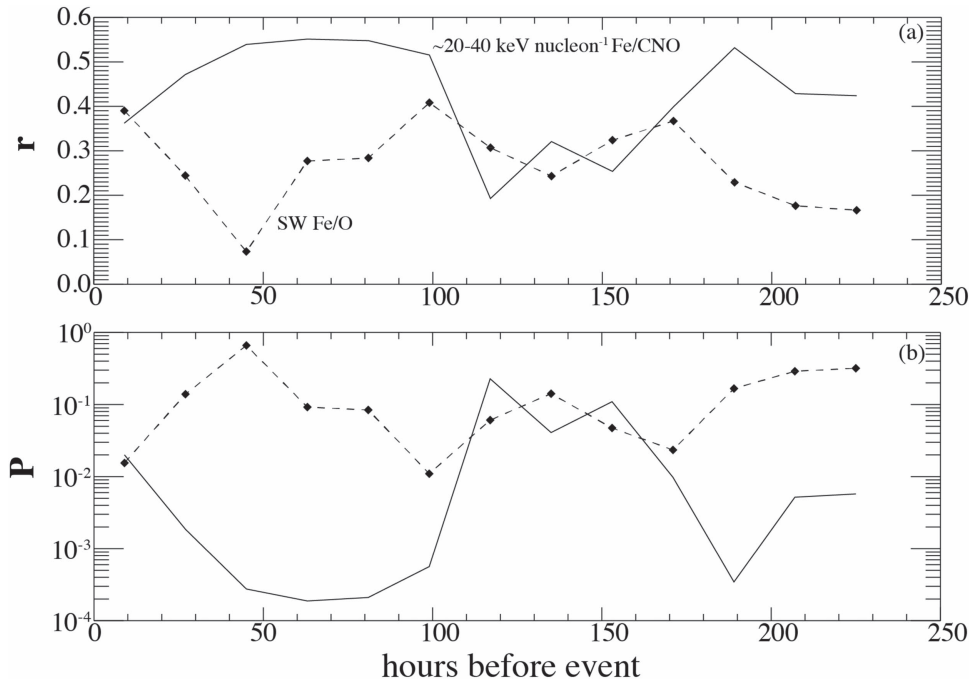


**Figure 9.** (a) The correlation coefficient for the Fe/CNO during the event at  $\sim 20\text{--}40$  keV nucleon $^{-1}$  when compared to both the upstream  $\sim 20\text{--}40$  keV nucleon $^{-1}$  Fe/CNO (solid line) and upstream solar wind Fe/O (dashed line) and (b) and associated probability of non-correlation.

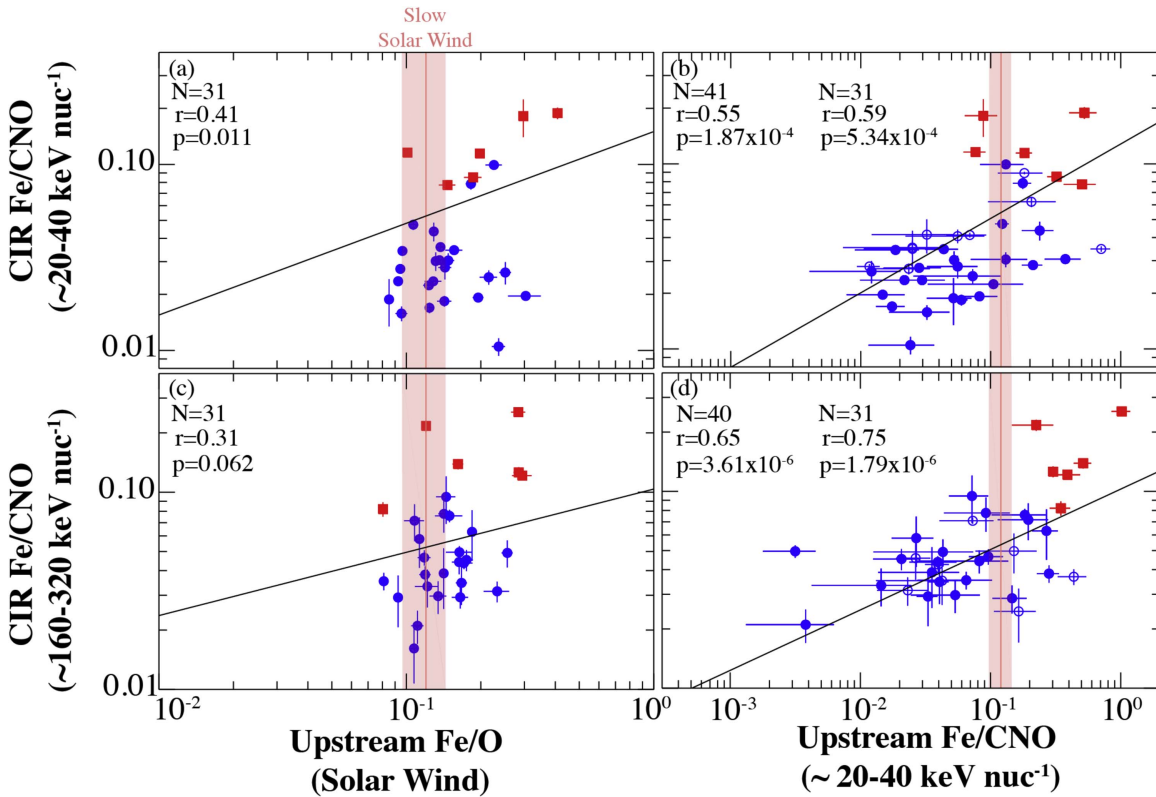


**Figure 10.** CIR Fe/CNO abundances at  $\sim 20\text{--}40$  keV nucleon $^{-1}$  (top panels) and  $\sim 160\text{--}320$  keV nucleon $^{-1}$  (bottom panels) plotted vs. left (a), (c): upstream solar wind Fe/O, and right (b), (d): upstream  $\sim 20\text{--}40$  keV nucleon $^{-1}$  Fe/CNO. The lines of best fit are plotted, and the events that occurred during solar maximum are shown by red squares, while solar minimum events are blue circles. In (b) and (d) the open symbols indicate the 10 events that are not included in the solar wind correlation. Also shown is the slow solar wind Fe/O ratio of  $0.120 \pm 0.024$  (von Steiger et al. 2000).

We find no relation between SW speed and Fe/CNO abundances, unlike Richardson et al. (1993). This leads us to conclude that there is no relationship between SW speed and abundance of ST heavy ions in CIRs, consistent with the

study by Mason et al. (2008). Furthermore, since the upstream ST populations are not identified with specific event types (i.e., CIR, quiet-time, SEP-like), we believe that they comprise a mix of ions from multiple sources, providing

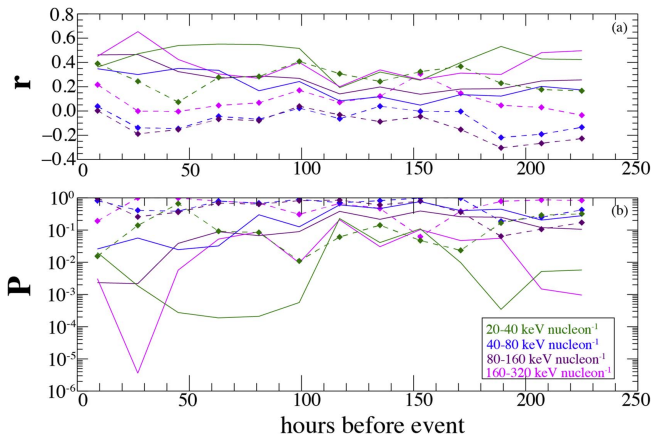


**Figure 11.** (a) The correlation coefficient and (b) corresponding probability for upstream solar wind Fe/O (dashed lines) and upstream Fe/CNO  $\sim 20\text{--}40$  keV nucleon $^{-1}$  (solid lines) with the CIR Fe/CNO at various energies (1)  $\sim 20\text{--}40$  keV nucleon $^{-1}$  (green) (2)  $\sim 40\text{--}80$  keV nucleon $^{-1}$  (blue) (3)  $\sim 80\text{--}160$  keV nucleon $^{-1}$  (purple) (4)  $\sim 160\text{--}320$  keV nucleon $^{-1}$  (magenta).

**Table 3**

Source Distance Upper Limit for  $\sim 20\text{--}320$  keV nucleon $^{-1}$  Fe/CNO Peak Correlation Times

$E(\text{keV nucleon}^{-1})$	Time Range	Field Line Distance	Radial Distance
$\sim 20\text{--}40$	45–99 hr	1.83–4.04 au	0.94–1.7 au
$\sim 40\text{--}80$	...	...	...
$\sim 80\text{--}160$	9–27 hr	0.55–1.65 au	0.29–0.85 au
$\sim 160\text{--}320$	18–35 hr	1.4–2.7 au	0.74–1.29 au
		$\mu = 2.03$ au	$\mu = 0.97$ au
		$\mu_w = 2.17$ au	

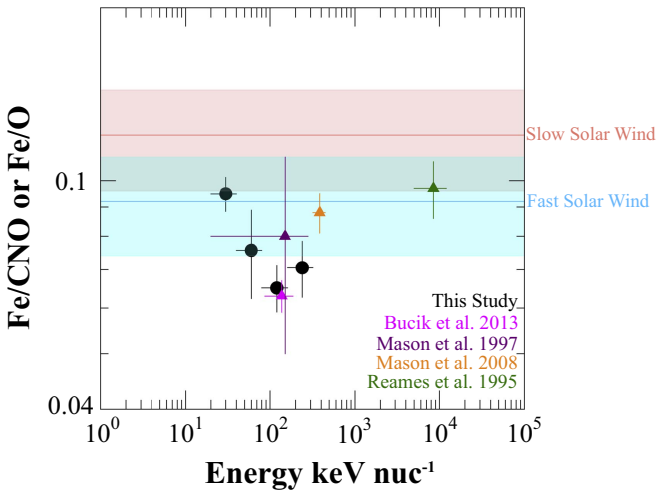


**Figure 12.** The average Fe/CNO in this study compared with Fe/O ratios found in other studies vs. energy. Also shown are the slow and fast solar wind Fe/O ratios:  $0.120 \pm 0.024$  and  $0.092 \pm 0.018$ , (von Steiger et al. 2000) respectively.

further evidence that the suprathermal tail is the source of local CIR events.

The correlation studies revealed statistically significant results for  $\sim 20\text{--}40$  keV nucleon $^{-1}$  upstream Fe/CNO versus  $\sim 20\text{--}320$  CIR Fe/CNO for extended time periods. The correlation with upstream SW Fe/O is not statistically significant. This indicates that the majority of the STs in CIRs are being accelerated from the lower-energy STs and not the solar wind. Thus, we conclude that, similar to those measured

in quiet times (i.e., Desai et al. 2006b; Dayeh et al. 2009), suprathermal heavy ion populations in CIRs derive their source material from the low-energy remnants of prior energetic particle activity, as also reported by Bućik et al. (2012).

### 4.3. Acceleration Location Limits

Recently, Ebert et al. (2012) studied the temporal profiles of suprathermal He in 73 CIRs and concluded that  $<1$  MeV nucleon $^{-1}$  CIR-associated energetic particles observed at 1 au are accelerated locally, whereas particles  $>1$  MeV nucleon $^{-1}$  are likely accelerated at CIR-driven shocks beyond Earth orbit. Chen et al. (2015) modeled PUIs in CIRs without shocks. They found gradual compressions and observed that velocity gradients can significantly accelerate PUIs at or inside of 1 au, leading to the formation of suprathermal tails. Mason et al. (2008) found a heliocentric distance of 1.3–2 au for  $\sim 320\text{--}450$  keV nucleon $^{-1}$  STs that had been accelerated out of the heated SW using the calculated maximum correlation time of approximately 4 days ( $r = 0.4$ ).

Figure 11 shows that for  $\sim 20\text{--}40$  keV nucleon $^{-1}$  and  $\sim 160\text{--}320$  keV nucleon $^{-1}$  there are two distinct peaks in the correlation coefficient. We observed the ST to become statistically significant again at  $\sim 8$  days, which is far too long to correspond to the same SW structure, as over a quarter of a solar rotation would have occurred from correlation time to event start (Gosling & Bame 1972). Since only the highest and lowest energy levels in this study displayed this strong correlation it is difficult to understand the physical mechanisms responsible for these longer time correlations.

Using the particle energy and maximum correlation time we now calculate limits for the source distances. Assuming no adiabatic deceleration and no scattering, and using the upstream correlation between  $\sim 20\text{--}40$  keV nucleon $^{-1}$  Fe/CNO upstream and  $\sim 20\text{--}320$  keV nucleon $^{-1}$  Fe/CNO in CIRs, we calculate an upper limit for the source distance using the peak correlation time. Table 3 shows the mean distance traveled by the ST particles detected in each of the four energy ranges. The particle energy is taken as the arithmetic mean of the lower and upper energy limits in each energy range. The distances were calculated using the time of maximum correlation in Figure 10, distances are not reported for  $\sim 40\text{--}80$  keV nucleon $^{-1}$  because the correlations do not exhibit statistical significance. The calculated average field line travel distance is  $\sim 2\text{--}2.2$  au, found by a standard mean and a weighted mean using the  $p$ -values for each time interval. Using the mean solar wind speed in the upstream region and the field line distances we find the upper limit for radial distance traveled beyond Earth for each energy range. We find that the average upper limit for radial distance, neglecting adiabatic deceleration and scattering affects, is  $\sim 1$  au beyond Earth orbit.

When adiabatic deceleration and realistic scattering is taken into account we expect the actual source distance to be even closer to Earth orbit. This is an indication that we are observing ST heavy ions upstream of CIRs being accelerated locally, consistent with the evidence for local acceleration ( $<1.5$  au) of ST heavy ions as reported by previous studies (e.g., Chottoo et al. 2000; Mason 2000; Ebert et al. 2012; Chen et al. 2015; Zhao et al. 2016).

We are thankful to many people who have worked on the EPACT instrumentation team at the University of Maryland, and at the Goddard Space Flight Center for the *Wind*/STEP

instrument. The solar wind data used in this study is in one-hour averages processed by the SWICS/SWIMS team using software version 4.07. Work at SwRI is partially supported by NSF grants AGS-1135432, AGS-1460118, NASA grants NNX14AP39G, NNX13AE07G, NNX13AI75G, and NASA contracts NNX10AT75G, NNN06AA01C.

### References

- Broiles, T. W., Desai, M. I., & McComas, D. J. 2012, *JGRA*, **117**, A03102
- Bučík, R., Mall, U., Korth, A., & Mason, G. M. 2012, *SoPh*, **281**, 411
- Chen, J. H., Schwadron, N. A., Möbius, E., & Gorby, M. 2015, *JGRA*, **120**, 9269
- Chotoo, K., Schwadron, N. A., Mason, G. M., et al. 2000, *JGRA*, **105**, 23107
- Dayeh, M. A., Desai, M. I., Dwyer, J. R., et al. 2009, *ApJ*, **693**, 1588
- Dayeh, M. A., Desai, M. I., Ebert, R. W., & Mason, G. M. 2016, in AIP Conf. Proc. 1720, SOLAR WIND 14: Proc. 14th Int. Solar Wind Conference (Melville, NY: AIP), 070001
- Desai, M. I., Dayeh, M. A., & Mason, G. M. 2009, in AIP Conf. Proc. 1183, 18th Annual Int. Astrophysics Conf., ed. X. Ao, R. Burrows, & G. P. Zank (Melville, NY: AIP), 11
- Desai, M. I., Mason, G. M., Dwyer, J. R., et al. 2000, *JGR*, **105**, 61
- Desai, M. I., Mason, G. M., Dwyer, J. R., et al. 2003, *ApJ*, **588**, 1149
- Desai, M. I., Mason, G. M., Mazur, J. E., & Dwyer, J. R. 2006, *ApJL*, **645**, L81
- Ebert, R. W., Dayeh, M. A., Desai, M. I., & Mason, G. M. 2012, *ApJ*, **749**, 73
- Fisk, L. A., & Lee, M. A. 1980, *ApJ*, **237**, 620
- Giacalone, J., Jokipii, J. R., & Kóta, J. 2002, *ApJ*, **573**, 845
- Gloeckler, G., Fisk, L. A., Mason, G. M., & Hill, M. E. 2008, in AIP Conf. Proc. 1039, Particle Acceleration and Transport in the Heliosphere and Beyond: 7th Annual Int. Astrophysics Conf., ed. G. Li et al. (Melville, NY: AIP), 367
- Gloeckler, G., Geiss, J., Balsiger, H., et al. 1992, *A&AS*, **92**, 267
- Gosling, J. T., & Bame, S. J. 1972, *JGRA*, **77**, 12
- Gosling, J. T. 1996, *ARA&A*, **34**, 35
- Jian, L., Russell, C. T., Luhmann, J. G., & Skoug, R. M. 2006, *SoPh*, **239**, 337
- Kucharek, H., Möbius, E., Li, W., et al. 2003, *JGRA*, **108**, 8040
- Mason, G. M. 2000, in AIP Conf. Proc. 528, Acceleration and Transport of Energetic Particles Observed in the Heliosphere, ed. R. A. Mewaldt et al. (Melville, NY: AIP), 234
- Mason, G. M., Leske, R. A., Desai, M. I., et al. 2008, *ApJ*, **678**, 1458
- Mason, G. M., Mazur, J. E., Dwyer, J. R., Reames, D. V., & von Rosenvinge, T. T. 1997, *ApJL*, **486**, L149
- Mazur, J. E., Mason, G. M.,Looper, M. D., Leske, R. A., & Mewaldt, R. A. 1999, *GeoRL*, **26**, 173
- McDonald, F. B., Teegarden, B. J., Trainor, J. H., & von Rosenvinge, J. H. 1976, *ApJL*, **203**, L149
- Reames, D. V. 1995, *AdSpR*, **15**, 41
- Richardson, I. G., Barbier, L. M., Reames, D. V., & Rosenvinge, T. T. 1993, *JGRA*, **98**, 13
- Van Hollebeke, M. A. I., McDonald, F. B., Trainor, J. H., & von Rosenvinge, T. T. 1978, *JGR*, **83**, 4723
- von Rosenvinge, T. T., Barbier, L. M., Karsch, J., et al. 1995, *SSRv*, **71**, 155
- von Steiger, R., Schwadron, N. A., Fisk, L. A., et al. 2000, *JGR*, **105**, 27217
- Zhao, L., Li, G., Ebert, R. W., et al. 2016, *JGRA*, **121**, 77